

## Supporting Information

### **Visible-light-driven Cr(VI) Reduction by Ferrocene-integrated Conjugated Porous Polymers via dual catalytic routes**

Yan Wang,<sup>a</sup> Weijie Zhang,<sup>a</sup> Yumin Yang,<sup>b</sup> Juntao Tang,<sup>\*,a</sup> Chunyue Pan,<sup>a</sup> You-Nian  
Liu,<sup>a</sup> Raed Abu-Reziq,<sup>c</sup> Guipeng Yu<sup>\*,a</sup>

<sup>a</sup> Hunan Key Laboratory of Micro & Nano Materials Interface Science, College of Chemistry and  
Chemical Engineering, Central South University, Changsha 410083, China.

<sup>b</sup> Northwestern Polytechnical University, Xian 710072, China

<sup>c</sup> Institute of Chemistry, The Hebrew University Jerusalem 9190401, Israel

\*Corresponding author:

Juntao Tang (E-mail: [reynardtang@csu.edu.cn](mailto:reynardtang@csu.edu.cn))

Guipeng Yu (E-mail: [gilbertyu@csu.edu.cn](mailto:gilbertyu@csu.edu.cn))

Postal address: College of Chemistry and Chemical Engineering, Central South University, 932  
South Lushan Road, Changsha 410083, Hunan, P. R. China.

## Section 1. Materials

4-Aminobenzonitrile, 4,4'-biphenyldicarboxaldehyde, anhydrous 1,4-dioxane and trifluoromethanesulfonic acid were gifted by energy Chemical. 1,1'-Ferrocenedicarboxaldehyde, and 1,3,5-tris(4-aminophenyl) benzene were purchased from Alfa Aesar Chemical Inc. All other solvents and reagents were purchased from commercial sources and used without further purification unless stated otherwise.

## Section 2. Methods

Fourier transform infrared (FTIR) spectra were recorded on a VARIAN 1000 FTIR spectrometer in the region of 500-4000  $\text{cm}^{-1}$  by potassium bromide pressed-disk technique. Solid-state  $^{13}\text{C}$  cross polarization magic angle spinning ( $^{13}\text{C}$  CP/MAS) NMR spectra were obtained on a Bruker Advance III 600 NMR spectrometer. The X-ray photoelectron spectra (XPS) were collected over Thermo ESCALAB 250 spectrometer with an Al-  $\text{K}\alpha$  X-ray source. Powder X-Ray Diffraction data were collected over the  $2\theta$  range 2-85° on a CPS120 Inel diffractometer equipped with Ni-filtered Cu  $\text{K}\alpha$  radiation (40 kV, 100 mA) at room temperature with a scan speed of 5°  $\text{min}^{-1}$ . The morphologies and microstructures were probed utilizing Scanning electron microscope (SEM, Nova NanoSEM 230). ESR spectra were recorded on a Bruker E500 spectrometer.  $\text{N}_2$  ad/desorption isotherms were performed at 77 K over Autosorb-iQ (Quantachrome) analyzer. The surfaces areas were calculated using the Brunauer-Emmett-Teller (BET) model range from 0.05 to 0.2 bar of  $\text{N}_2$  adsorption isotherms. The pore size distribution curves were derived from the  $\text{N}_2$  adsorption isotherms using nonlocalized density function theory (NLDFT). The NLDFT method is based on a molecular model for gas adsorption in porous solids. It is assumed that the external surface area is much smaller than the surface area of the pores, and the experimental adsorption isotherm measured is the aggregate of the isotherms for the individual pores that make up the pore structure of the solid, that is the experimental isotherm is the integral of the single pore isotherm multiplied by the pore size distribution. The UV/vis diffuse reflectance spectroscopy (DRS) were recorded on a

U-4100 spectrometer (Hitachi Limited, Japan). Photoluminescence (PL) spectra were recorded on an Edinburgh FLS1000 spectrophotometer.

Electrochemical measurements of samples were carried out at room temperature in a three-electrode cell. Ag/AgCl/KCl(saturated) electrode and Pt electrode were used as reference electrode and the counter, respectively. The catalysts were modified on glassy carbon electrode (diameter is 3 mm) as the working electrode. 5 mg of catalyst and 10  $\mu$ L of Nafion solution were dispersed in mixed solution of ethanol (792  $\mu$ L) and distilled water (198  $\mu$ L) by sonicating for 30 min to form a homogeneous catalyst ink. Then, 20  $\mu$ L the catalyst ink was uniformly deposited on glassy carbon electrode to act as the working electrode. Before cyclic voltammetry experiments, the electrolyte (0.1 M  $\text{Bu}_4\text{NPF}_6$ ) was bubbled with  $\text{N}_2$  for 10 min and then cyclic voltammetry was done at a scan rate of 50 mV/s. The sample preparation process of Electrochemical impedance spectroscopy (EIS), photocurrent and cyclic voltammetry test are the same. For EIS and photocurrent test, the electrolyte is changed to 0.4 M  $\text{Na}_2\text{SO}_4$ . EIS characterizations were carried out at open circuit potential. For photocurrent test, the catalysts were modified on conductive glass of 1 cm  $\times$  0.5 cm as working electrode and transient photocurrent responses was recorded at visible light source ( $\lambda=420\pm 10$ ). Electrostatic potential map was carried out by Standard ab initio molecular orbital theory and density functional theory calculations with the Gaussian 09 software package and Gauss View visualization program. In determination of geometric optimization, HF method with 631++G(d) basis set were used.

### **Section 3. Experimental Section**

#### **Preparation of 2,4,6-tris(4-aminophenyl)-1,3,5-triazine**

4-aminobenzonitrile (13 mmol, 1.544 g) were added in a 25 mL two-necked flask. After leaving in an ice bath for 20 min, trifluoromethanesulfonic acid (4 mL) was added to the reaction system. The mixture was stirred about 20 min in an ice bath and then continued for 24 h at room temperature. Then distilled water and 2 M NaOH solution was added dropwise to the reaction system until the solution was neutral. The

product was obtained by filtration and then dried for 12 h via the vacuum freeze-drying (70 °C) in a yield of 78%.

#### **Preparation of Fc-CPP-1**

Under the protection of N<sub>2</sub>, 1,1'-ferrocenedicarboxaldehyde (0.145g, 0.6 mmol), 2,4,6-tris(4-aminophenyl)-1,3,5-triazine (0.142 g, 0.4 mmol) anhydrous dioxane (5 mL) and acetic acid (0.5 mL) were added in a glass flask. Then the mixture was degassed by three freeze-pump-thaw cycles and warmed to room temperature. And then the tube was kept at 120 °C in oil bath with stirring for 72 h, following which the reaction was stopped and cooled to room temperature. The precipitate was collected by filtration and was washed with dimethyl formamide. Subsequently, the obtained solid was further Soxhlet extracted using tetrahydrofuran for 24 h. The product was dried at 100 °C under vacuum for 24 h to obtain red powder in a yield of 62%.

#### **Preparation of Fc-CPP-2**

Under the protection of N<sub>2</sub>, 1,1'-ferrocenedicarboxaldehyde (0.145g, 0.6 mmol), 1,3,5-tris(4-aminophenyl) benzene (0.141 g, 0.4 mmol), anhydrous dioxane (5 mL) and acetic acid (0.5 mL) were added in a glass flask. The synthesis condition of Fc-CPP-2 was the same as that of Fc-CPP-1. Then white product was obtained in a yield of 65%.

#### **Preparation of Bp-CPP-1**

Under the protection of N<sub>2</sub>, 4,4'-biphenyldicarboxaldehyde (0.126 g, 0.6 mmol), 2,4,6-tris(4-aminophenyl)-1,3,5-triazine (0.142 g, 0.4 mmol), anhydrous dioxane (5 mL) and acetic acid (0.5 mL) were added in a glass flask. The synthesis condition of Bp-CPP-1 was the same as that of Fc-CPP-1. Then yellow product was obtained in a yield of 63%.

#### **Photocatalytic reduction of Cr(VI) to Cr(III) using CPPs**

The photocatalytic reduction of Cr(VI) was performed over CPPs in N<sub>2</sub> atmosphere

under visible light irradiation of a 14 W LED lamp (0.20 W/cm<sup>2</sup>). In a 25 mL one-necked round-bottom flask, 6 mg CPPs were added into 6 ml of Cr(VI) solution (K<sub>2</sub>CrO<sub>7</sub> in H<sub>2</sub>O, 25 mg/L). The reaction mixture was protected with an N<sub>2</sub> balloon (~0.1MPa). The Cr content in the reaction solution was determined by the DPC method using the UV-vis spectroscopy.<sup>[4]</sup> The photocatalytic efficiency was determined by dividing C<sub>t</sub>/C<sub>0</sub>, where C<sub>t</sub> is the remained Cr(VI) concentration and C<sub>0</sub> is the starting Cr(VI) concentration.

### **Recycle experiments for photocatalytic reduction of Cr(VI) to Cr(III) using CPPs**

In a 25 mL one-necked round-bottom flask, 6 mg CPPs were added into 6 ml of Cr(VI) solution (K<sub>2</sub>CrO<sub>7</sub> in H<sub>2</sub>O, 25 mg/L). The reaction mixture was stirred under the irradiation of 14 W LED lamp (0.20 W/cm<sup>2</sup>) at room temperature in the presence of N<sub>2</sub> balloon (~0.1MPa). The Cr content in the reaction solution was determined by the DPC method using the UV-vis spectroscopy. After each cycle, the CPPs was centrifuged at 10000 rpm for 10 min by a micro centrifuge. The CPPs sediment was collected, washed several times with water and ethanol, dried under vacuum oven at 70 °C for overnight and was reused for next cycle.

### **Indication of H<sub>2</sub>O<sub>2</sub> after completing the reaction**

The H<sub>2</sub>O<sub>2</sub> amount coming out during the process was determined by redox titration with KMnO<sub>4</sub> (0.2 mmol L<sup>-1</sup>) with the addition of 5 mL of H<sub>2</sub>SO<sub>4</sub> solution (1 mol L<sup>-1</sup>). When the color of solution became pink after adding KMnO<sub>4</sub> solution and the color was kept for 1 min, the concentration of KMnO<sub>4</sub> solution was equivalent to the concentration of H<sub>2</sub>O<sub>2</sub>.

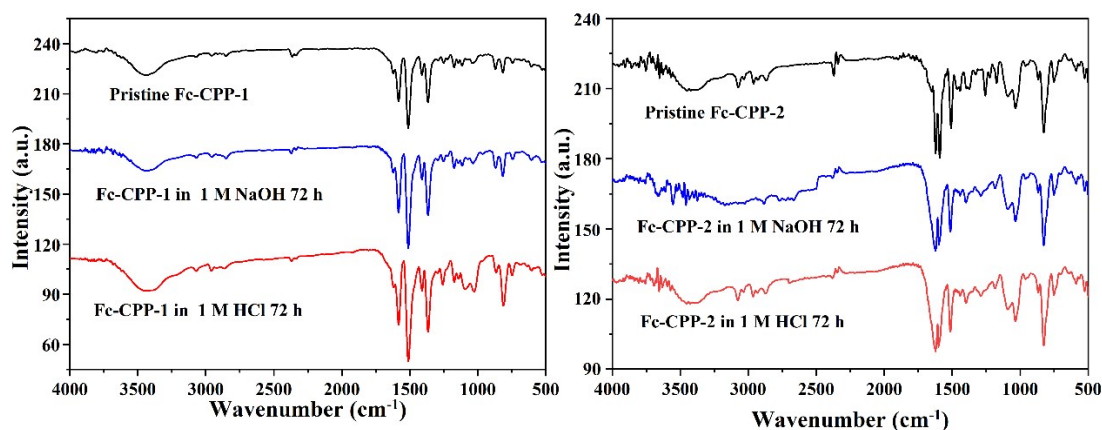


**Fig. S1** FTIR spectra of Fc-CPP-1 and Fc-CPP-2 after immersing in NaOH and HCl.

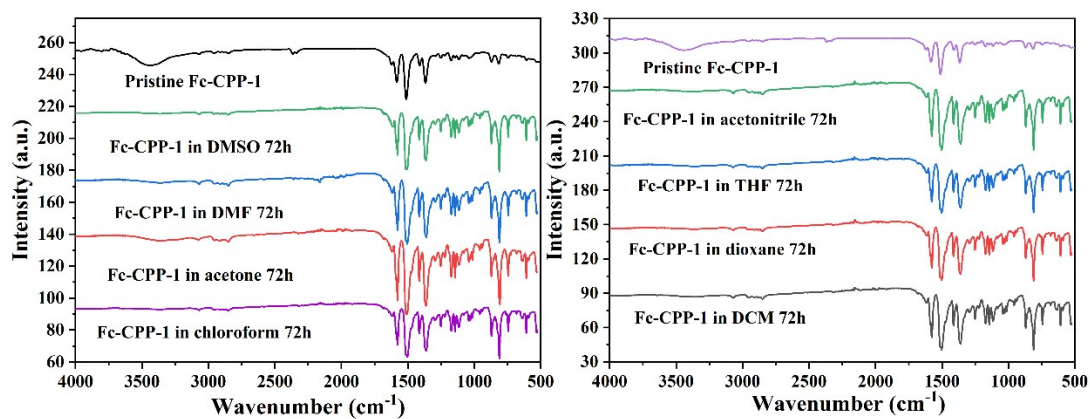


**Fig. S2** FTIR spectra of Fc-CPP-1 after immersing in common organic solvents.

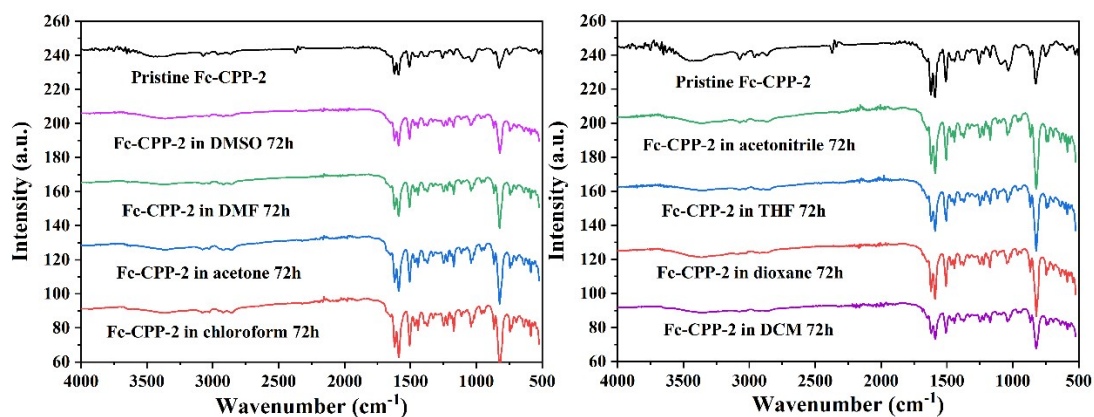


**Fig. S3** FTIR spectra of Fc-CPP-2 after immersing in common organic solvents.

In order to investigate the stability of Fc-CPPs, we immersed them in 1 M HCl and 1 M NaOH and common organic solvents (dimethyl sulfoxide (DMSO), N,N-

Dimethylformamide (DMF), acetone, chloroform, acetonitrile, tetrahydrofuran (THF), dioxane, dichloromethane) for 72 hours. Then the soaked samples are dried and confirmed by FTIR. If Fc-CPPs are unstable in these solvents, monomers will be precipitated after dissolution, so the FTIR spectra will show peaks of aldehyde groups ( $\sim 1672\text{cm}^{-1}$ ) and amino groups ( $3430\text{-}3208\text{cm}^{-1}$ ). It can be seen from Fig.S2-Fig.S4, that compared with the pristine sample, the FTIR spectra of the soaked samples are basically unchanged (and no aldehyde peaks and amino peaks appear), so they are stable in these solvents.

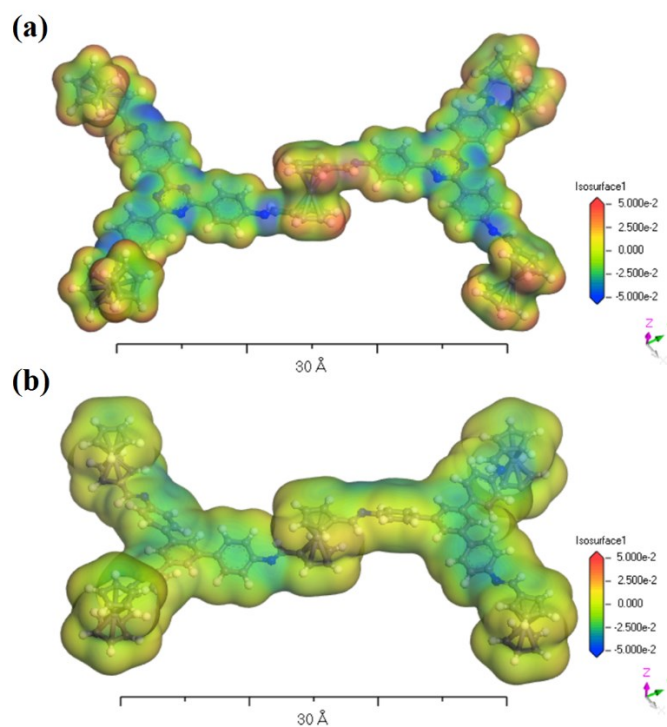


**Fig. S4** Electrostatic potential map of oligomer models of Fc-CPPs.

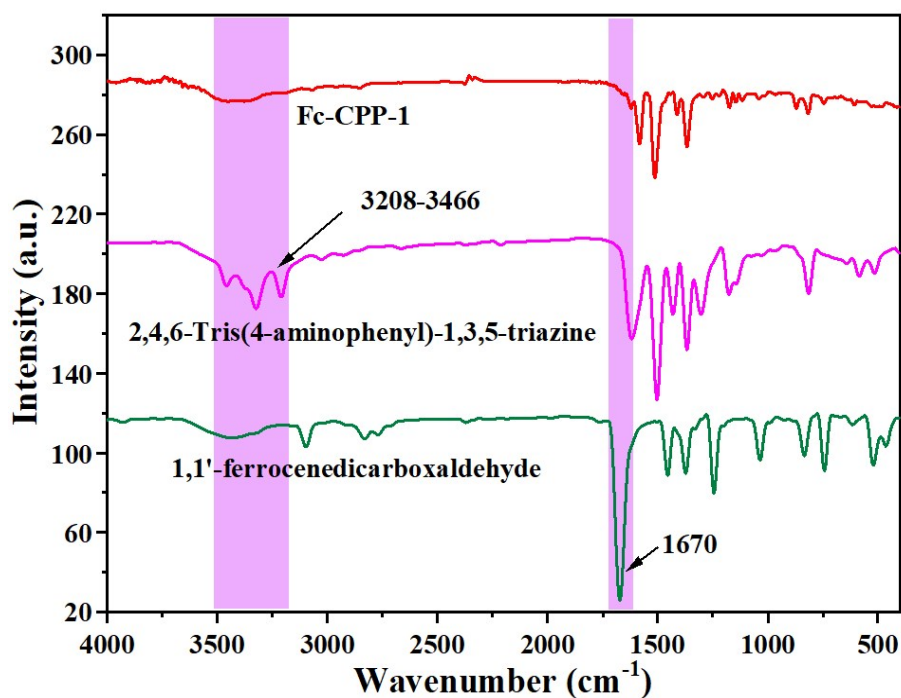


**Fig. S5** FTIR spectra of Fc-CPP-1 and monomers. The apparent bands at  $1670\text{cm}^{-1}$  correspond to the C=O. The peak is assigned to the  $\text{-NH}_2$  stretching vibration nearing  $3208\text{-}3466\text{ cm}^{-1}$ . In FTIR spectra of Fc-CPP-1, both types of stretching vibration bands disappear, indicating the almost complete conversion of the C=O and  $\text{-NH}_2$  bond.

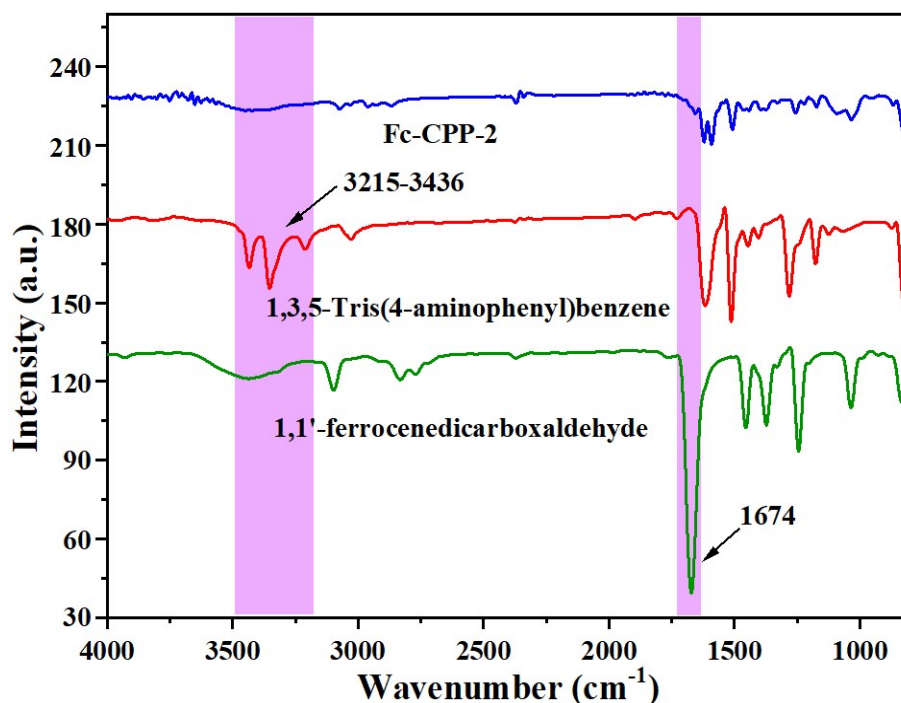


**Fig. S6** FTIR spectra of Fc-CPP-2 and monomers. The apparent bands at  $1674\text{cm}^{-1}$  correspond to the C=O. The peak is assigned to the  $\text{-NH}_2$  stretching vibration nearing  $3215\text{-}3436\text{ cm}^{-1}$ . In FTIR spectra of Fc-CPP-2, both types of stretching vibration

bands disappear, indicating the almost complete conversion of the C=O and -NH<sub>2</sub> bond.

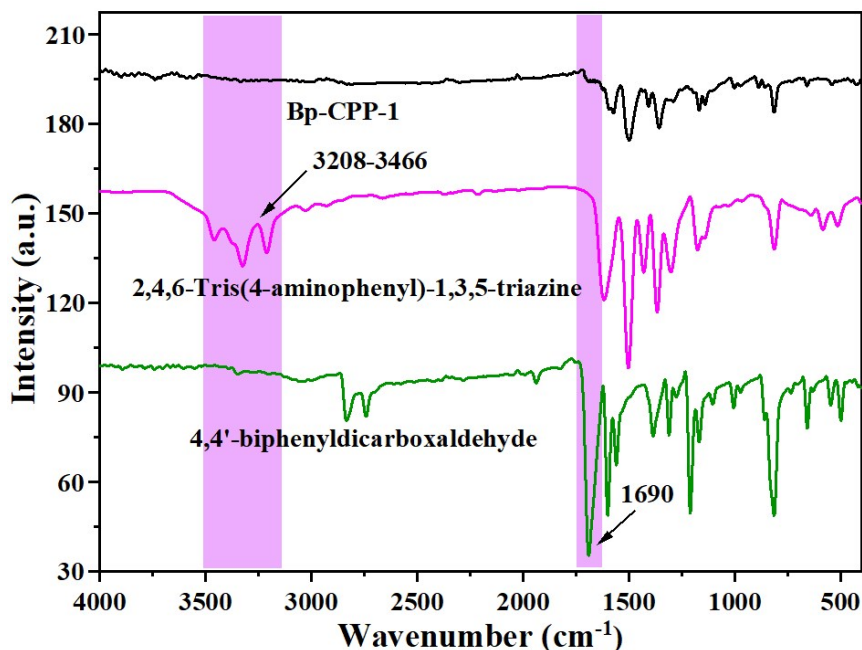


**Fig. S7** FTIR spectra of Bp-CPP-1 and monomers. The apparent bands at 1690 cm<sup>-1</sup> correspond to the C=O. The peak is assigned to the -NH<sub>2</sub> stretching vibration nearing 3208-3466 cm<sup>-1</sup>. In FTIR spectra of Bp-CPP-1, both types of stretching vibration bands disappear, indicating the almost complete conversion of the C=O and -NH<sub>2</sub> bond.

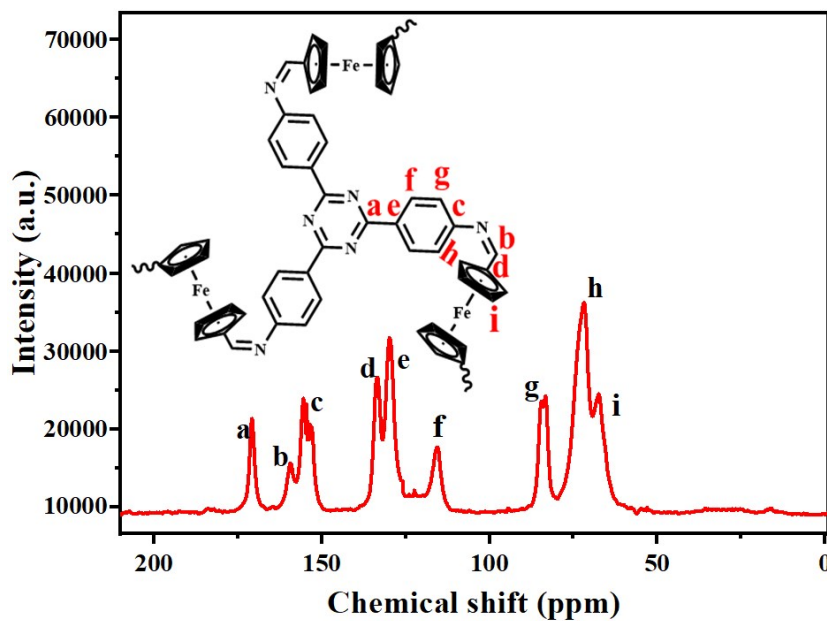


**Fig. S8** Solid <sup>13</sup>C CP/MAS NMR spectrum of Fc-CPP-1.

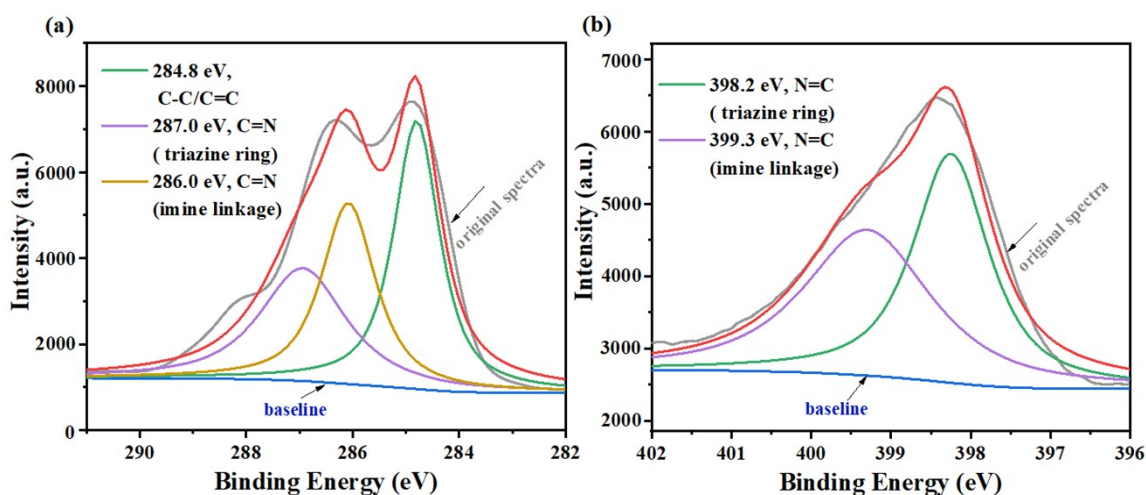


Fig. S9 C<sub>1s</sub> (a) and N<sub>1s</sub> (b) of XPS spectra for Fc-CPP-1. According to XPS, the local chemical states of the elemental in the polymers are identified. The C<sub>1s</sub> XPS spectrum of Fc-CPP-1 is shown in Fig. S8 (a), which can be fitted with three peaks at 284.7 eV (C-C/C=C bonds), 287.0 eV (C=N bonds, triazine ring) and 386.0 eV (C=N bonds, imine linkage). In the N<sub>1s</sub> spectrum (Fig. S8 (b)), there are two peaks. The peak at 398.2 eV is assigned to N=C bonds on triazine ring and the peak at 399.3 eV is indexed to N=C bonds formed by Schiff base reaction. These results further demonstrate the polymerization proceeded successfully.

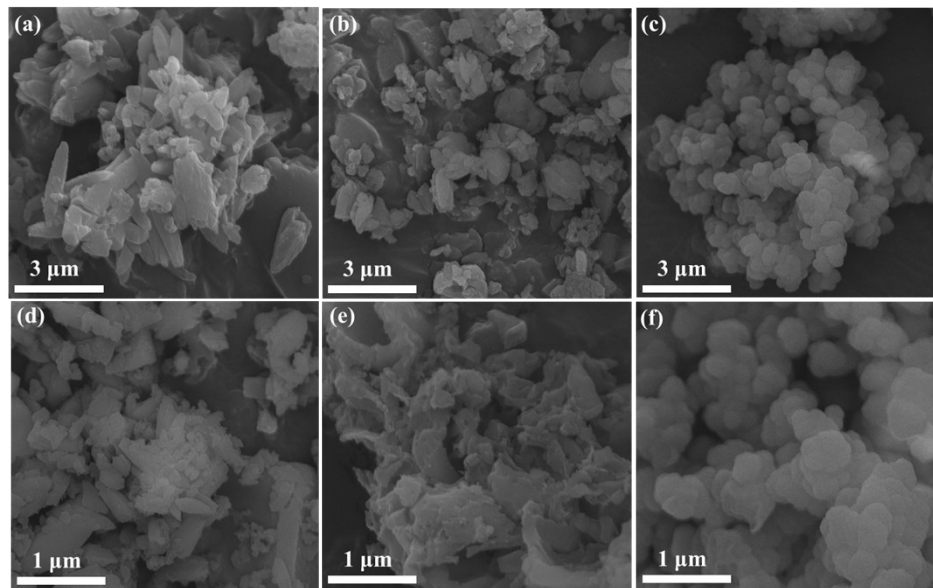


Fig. S10 The SEM images of (a, d) Fc-CPP-1, (b, e) Fc-CPP-2 and (c, f) Bp-CPP-1.

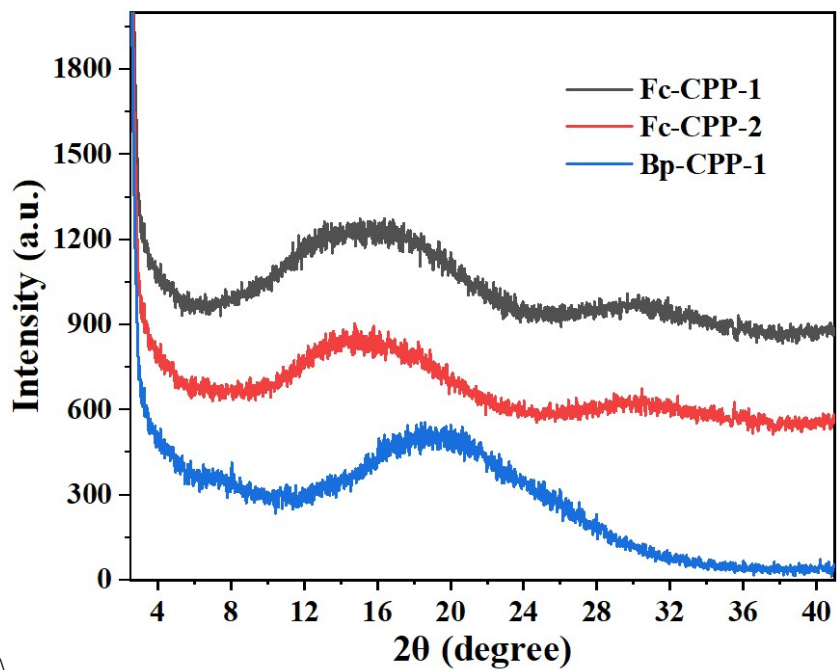


Fig. S11 PXRD patterns of Fc-CPPs and Bp-CPP-1.

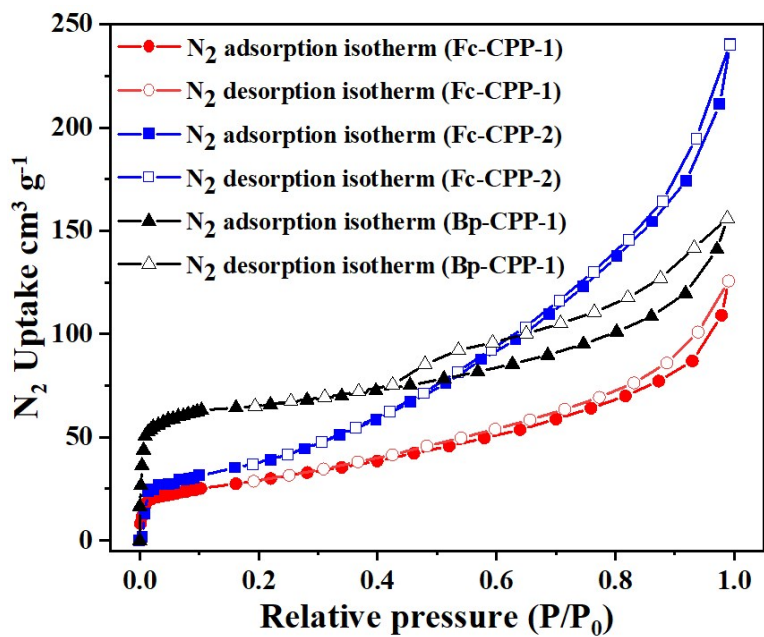


Fig. S12 N<sub>2</sub> sorption isotherms of Fc-CPPs and Bp-CPP-1 at 77 K.

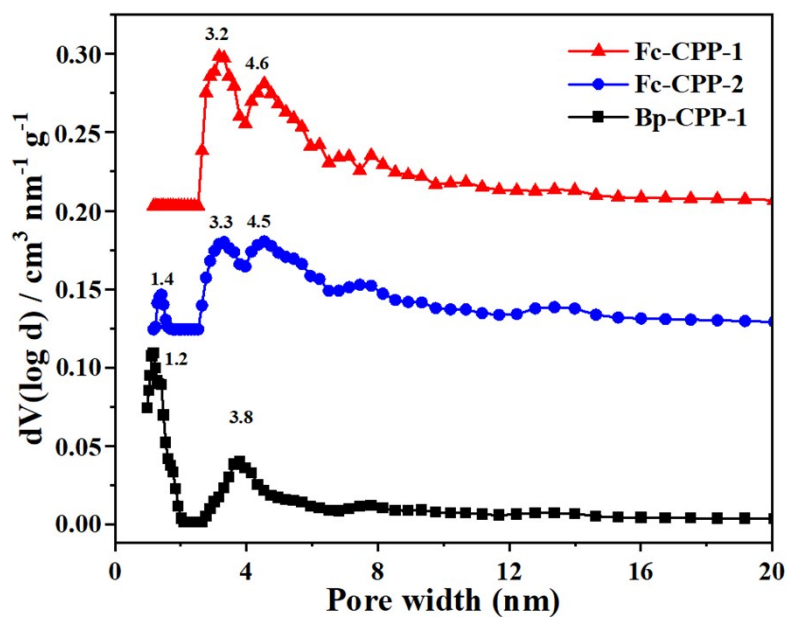


Fig. S13 NLDFT pore size distribution curves of Fc-CPPs and Bp-CPP-1.

Table S1 Pore parameters for CPPs.

Sample	$S_{\text{BET}}$ ( $\text{m}^2 \text{g}^{-1}$ )	$V_{\text{Total}}$ ( $\text{cm}^3 \text{g}^{-1}$ )	$V_{\text{Meso}}$ ( $\text{cm}^3 \text{g}^{-1}$ )	$V_{\text{Meso}}/V_{\text{Total}}$ (%)	Dominant Pore Size (nm)
Fc-CPP-1	251	0.488	0.429	88	3.2, 4.6
Fc-CPP-2	256	0.508	0.468	87	3.3, 4.5
Bp-CPP-1	249	0.441	0.143	32	1.2, 3.8

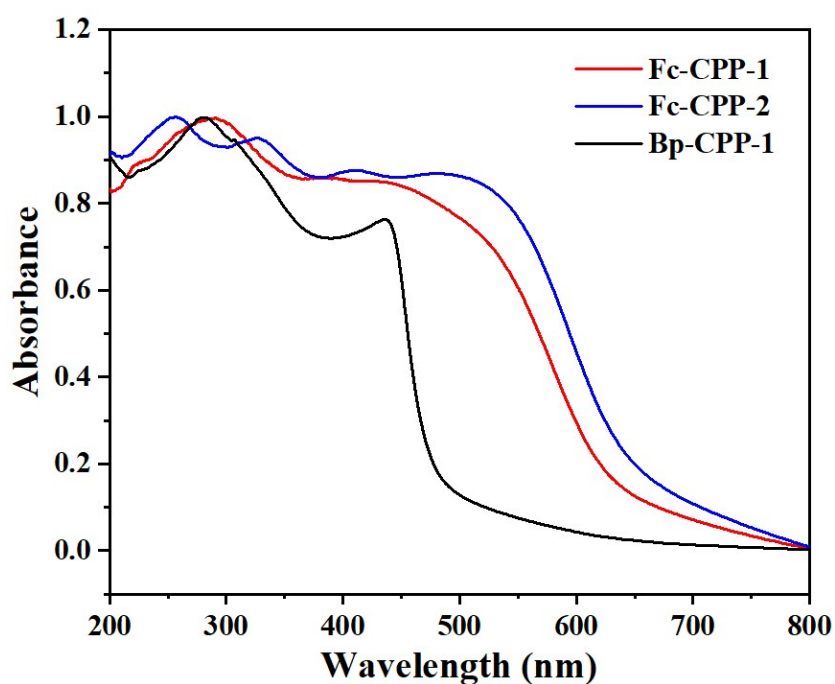
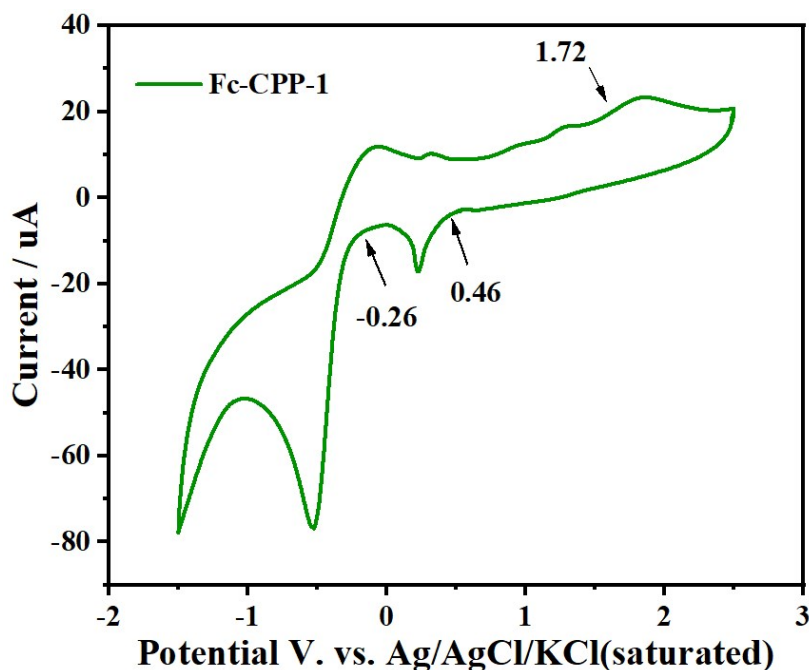
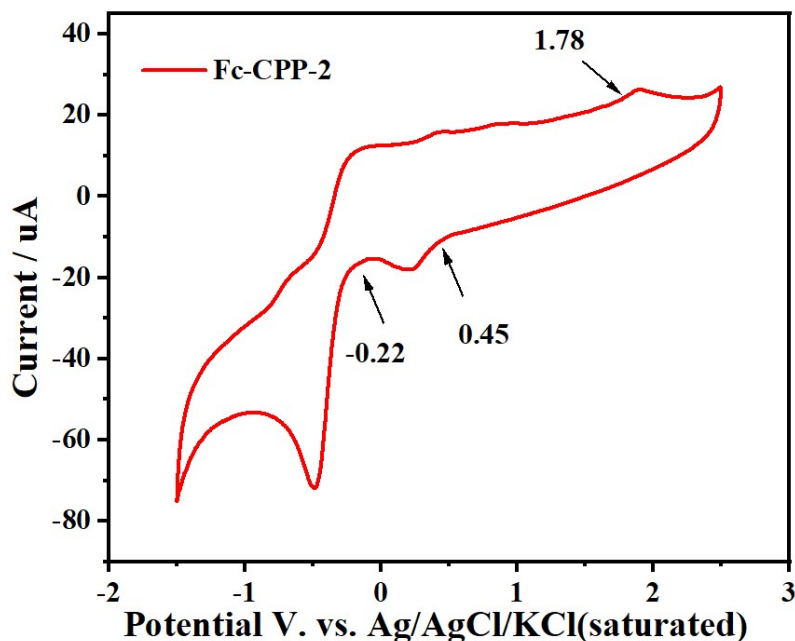


Fig. S14 Normalized UV-vis diffuse reflectance spectra of Fc-CPPs and Bp-CPP-1.



**Fig. S15** Cyclic voltammetry of Fc-CPP-1. As shown in Fig.S15, Fc-CPP-1 show two reduction peaks. The peak at  $\sim 0.46$  V (vs Ag/AgCl/KCl(saturated)) can be assigned to the reversible Fc/Fc<sup>+</sup> couple. The peak at  $\sim -0.26$  V (vs Ag/AgCl/KCl(saturated)) can be attributed to the reduction potential of the overall polymer backbone.



**Fig. S16** Cyclic voltammetry of Fc-CPP-2. As shown in Fig.S16, Fc-CPP-2 show two reduction peaks. The peak at  $\sim 0.45$  V (vs Ag/AgCl/KCl(saturated)) can be assigned to the reversible Fc/Fc<sup>+</sup> couple. The peak at  $\sim -0.22$  V (vs Ag/AgCl/KCl(saturated)) can be attributed to the reduction potential of the overall polymer backbone.

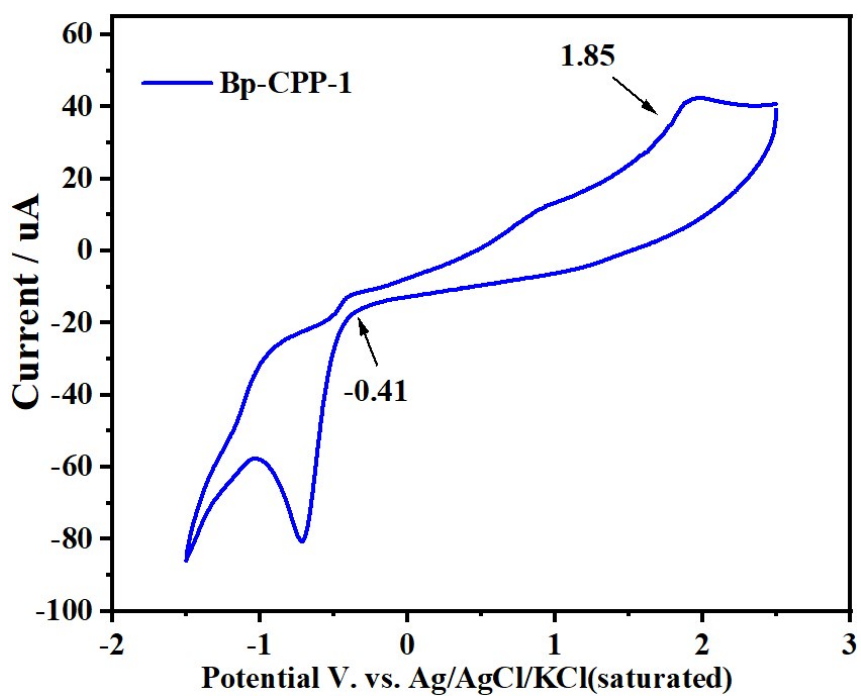


Fig. S17 Cyclic voltammetry of Bp-CPP-1.

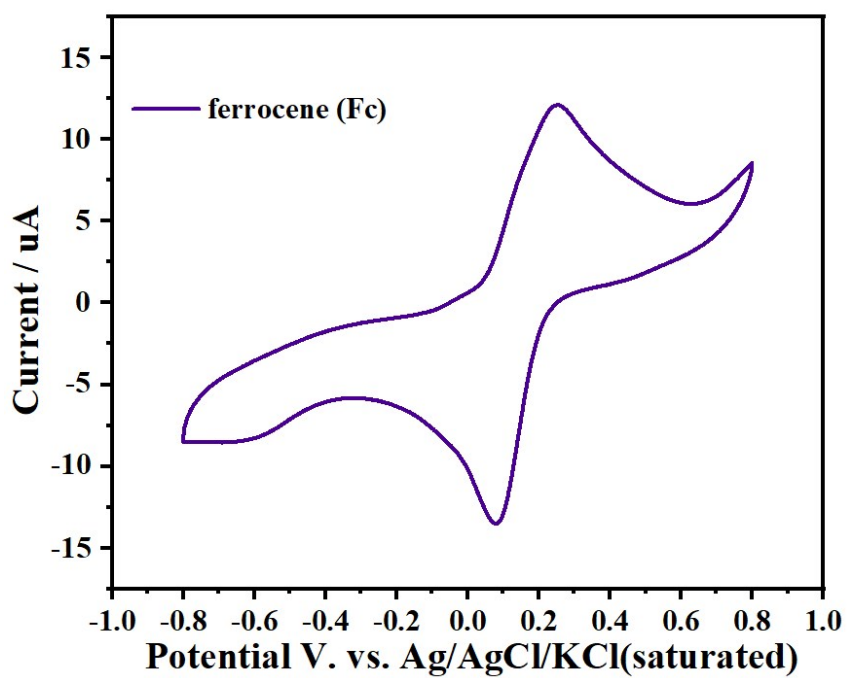


Fig. S18 Cyclic voltammetry of ferrocene.

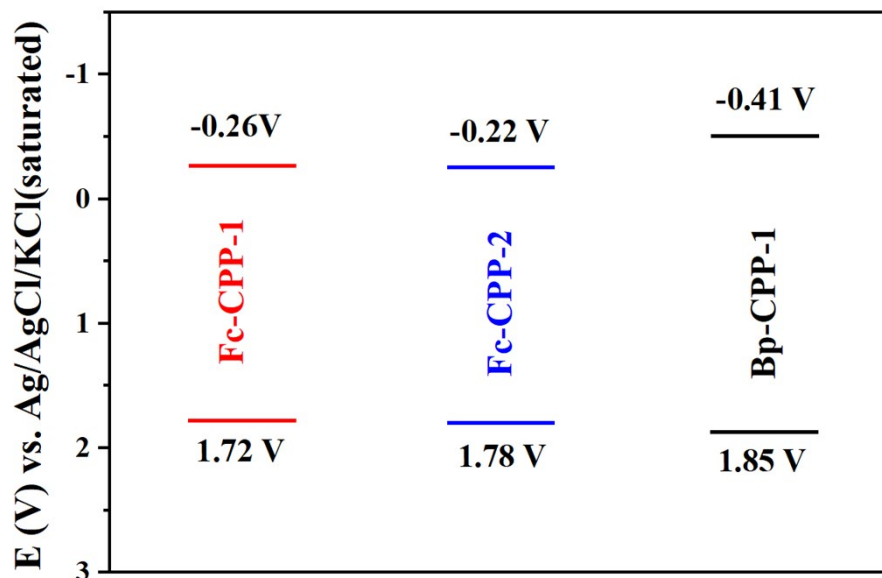


Fig. S19 LUMO and HOMO of Fc-CPPs and Bp-CPP-1.

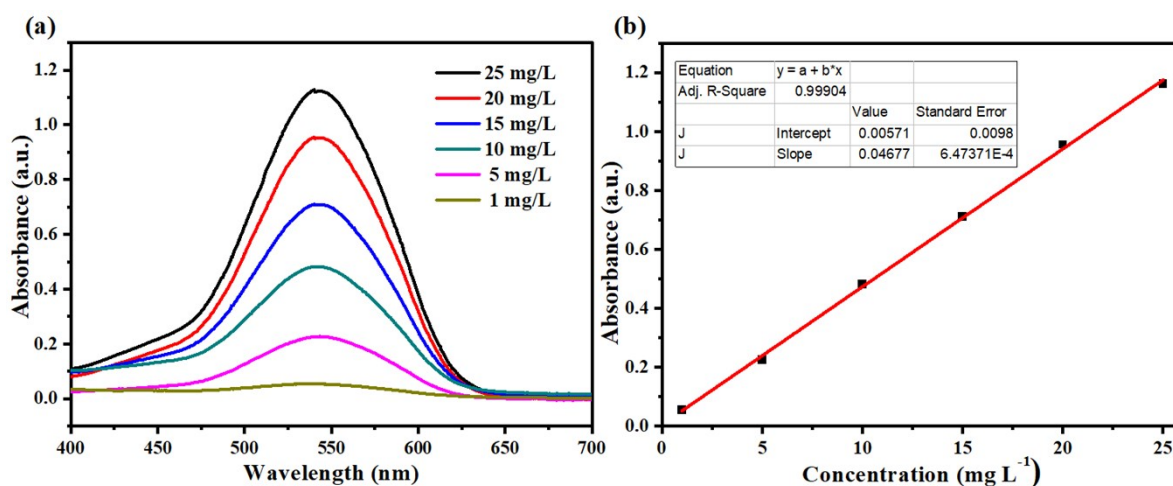
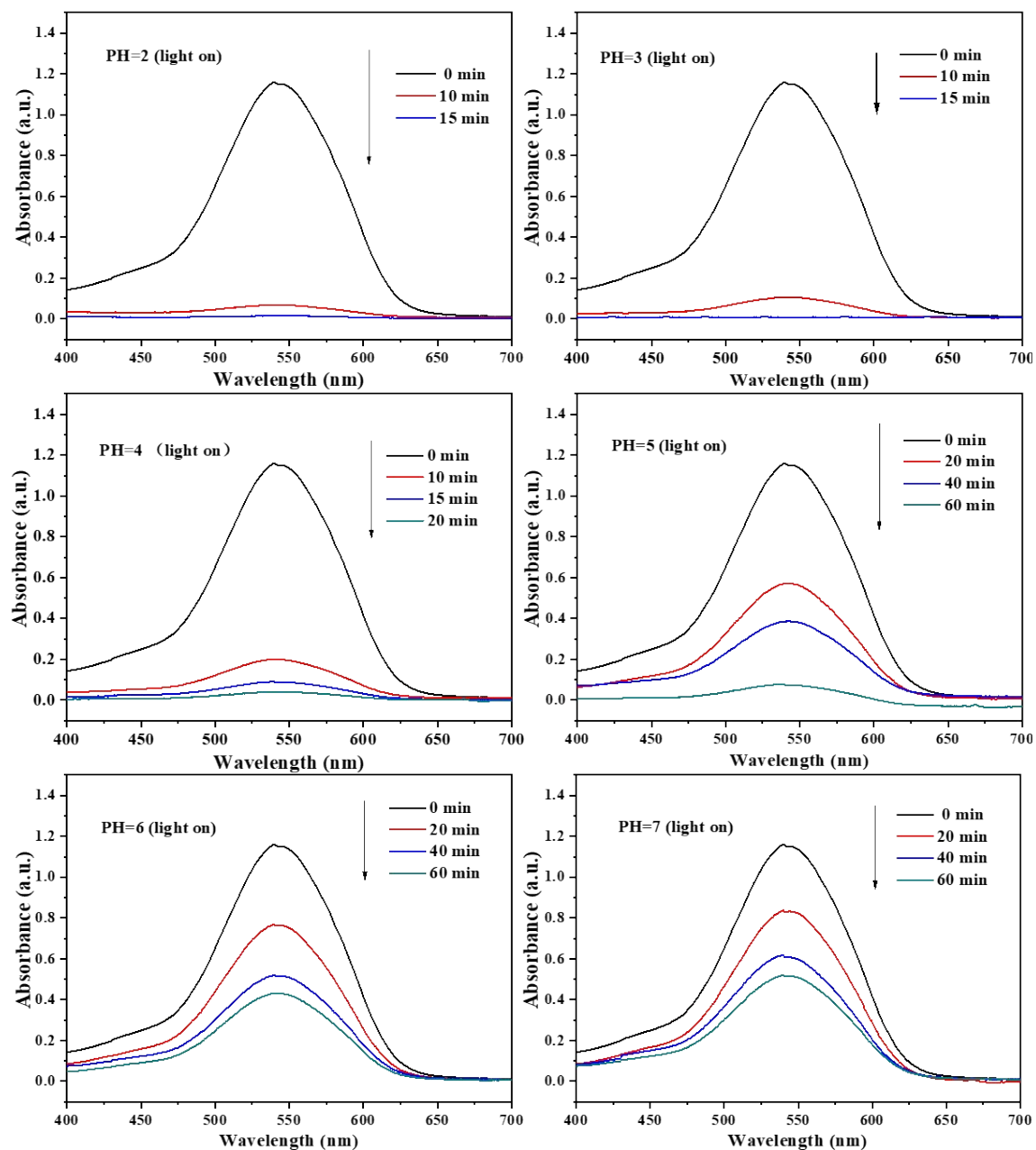
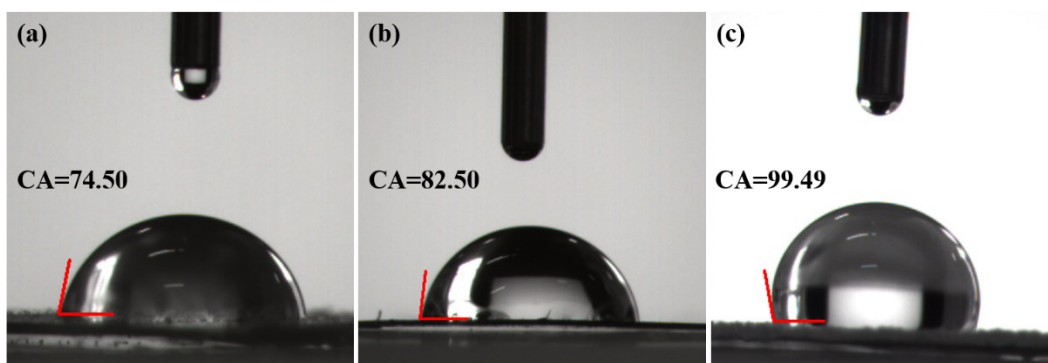


Fig. S20 (a) Absorption spectral pattern of DPC-Cr(VI) complex solutions at different Cr(VI) concentration. (b) Standard curves of the UV-vis absorption spectra of DPC-Cr(VI) complex solutions.



**Fig. S21** Time-dependent absorption spectral pattern of DPC-Cr(VI) complex solutions after reduction over Fc-CPP-1 at different pH values. (the initial concentration of Cr(VI) ( $K_2CrO_7$  in  $H_2O$ ) :  $25\text{ mg L}^{-1}$ ; Fc-CPP-1:  $1.0\text{ g L}^{-1}$ ).



**Fig. S22** Contact angle of Fc-CPP-1 (a), Fc-CPP-2 (b) and Bp-CPP-1(c). It can be seen from Fig. S13 that the contact angle of Fc-CPPs is less than  $90^\circ$ , so the solid surface is hydrophilic, and the aqueous solution is easier to wet the solid.

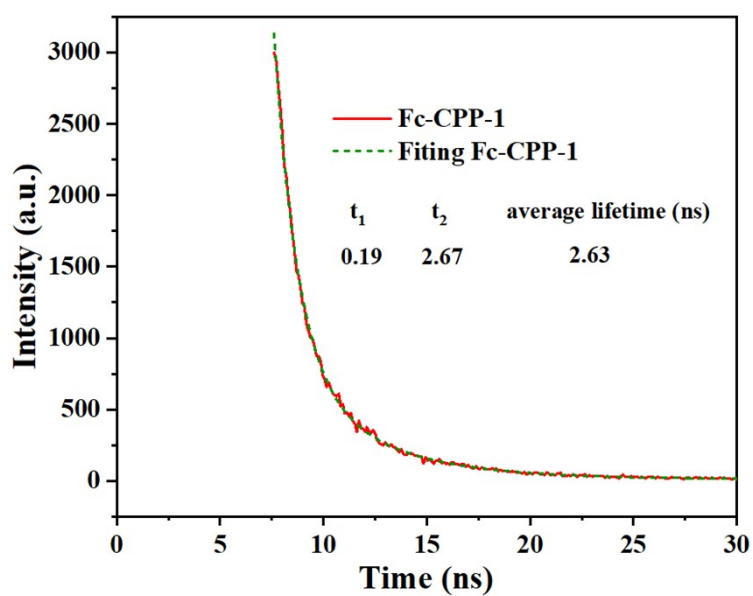


**Fig. S23** Time-resolved photoluminescence decay spectra of Fc-CPP-1.

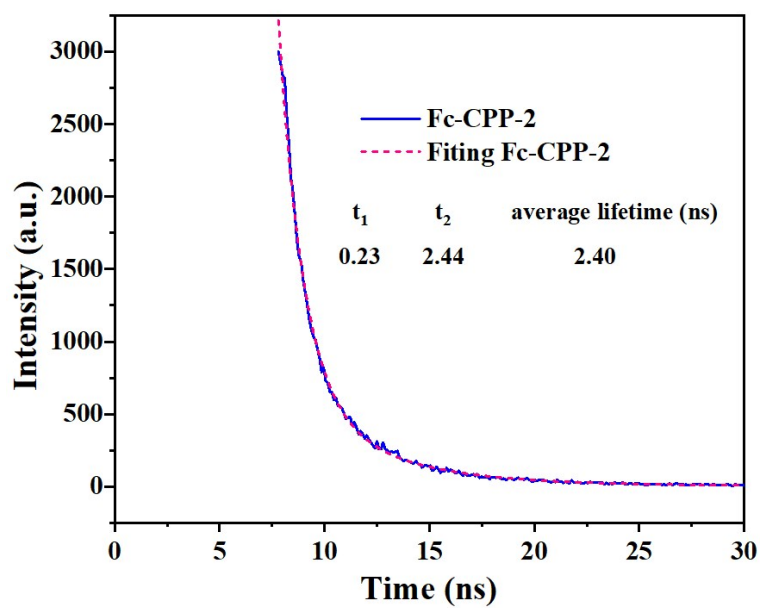


**Fig. S24** Time-resolved photoluminescence decay spectra of Fc-CPP-2.

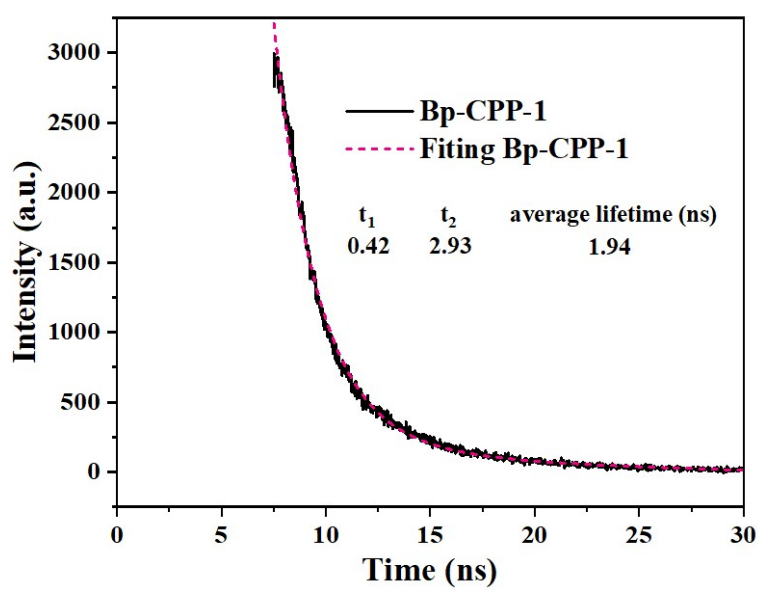


**Fig. S25** Time-resolved photoluminescence decay spectra of Bp-CPP-1.

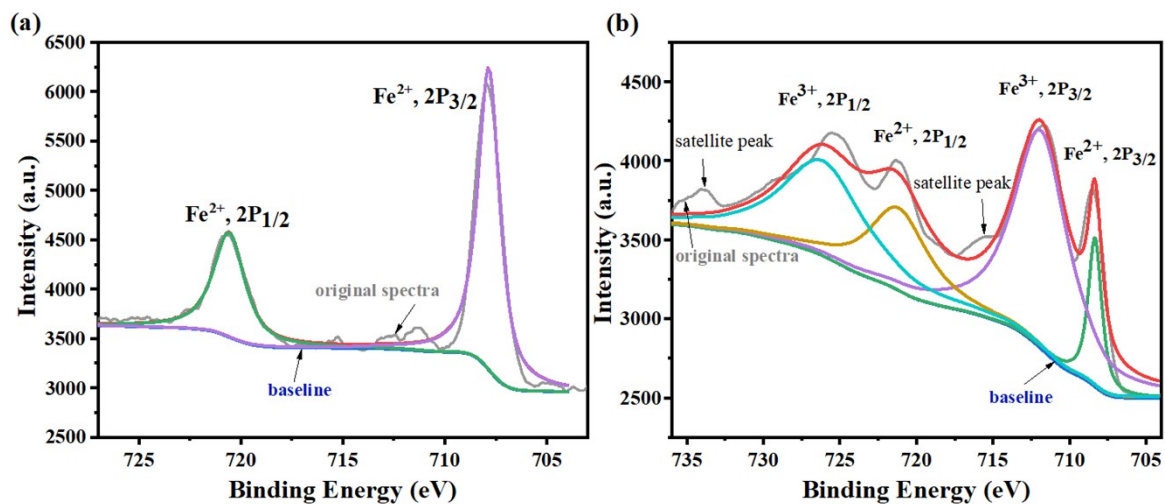


**Fig. 26** XPS of Fe 2p spectra for (a) pristine Fc-CPP-1 and (b) Fc-CPP-1 after reaction under dark.

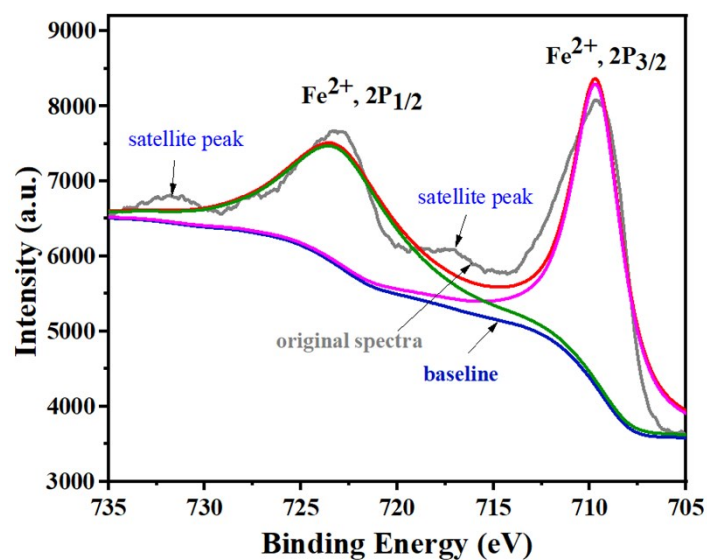


**Fig. 27** XPS of Fe 2p spectra for Fc-CPP-1 after reaction under visible light irradiation.

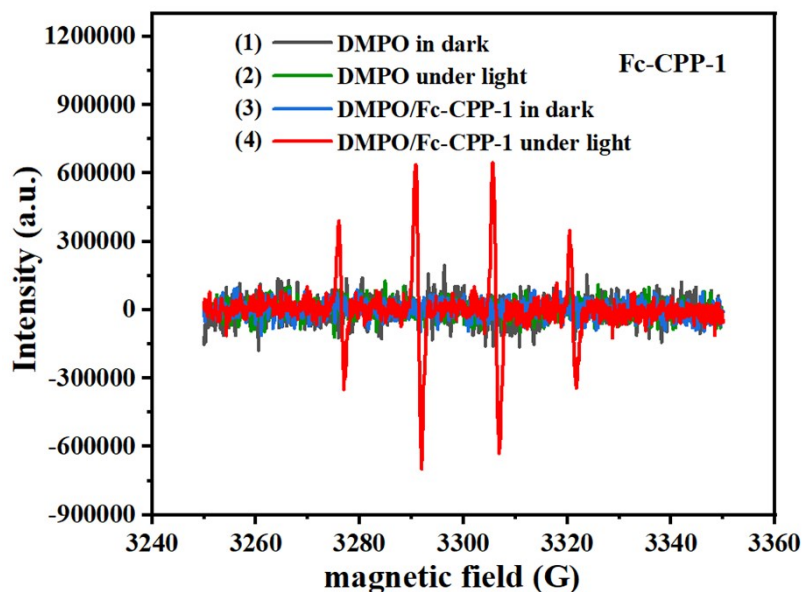


**Fig. S28** ESR spectra for DMPO-•OH in 1) distilled water of DMPO before irradiation, 2) distilled water of DMPO after irradiation, 2) distilled water of DMPO in the presence of Fc-CPP-1 before irradiation, and d) distilled water of DMPO in the presence of Fc-CPP-1 after irradiation. ESR spectroscopy were performed by employing 5,5-dimethyl-1-pyrroline N-oxide (DMPO) as a spin trapping agent to detect •OH. Characteristic four peaks of DMPO-•OH adduct (peak area = 1:2:2:1) are observed for Fc-CPP-1 under visible light irradiation, demonstrating •OH species are generated.

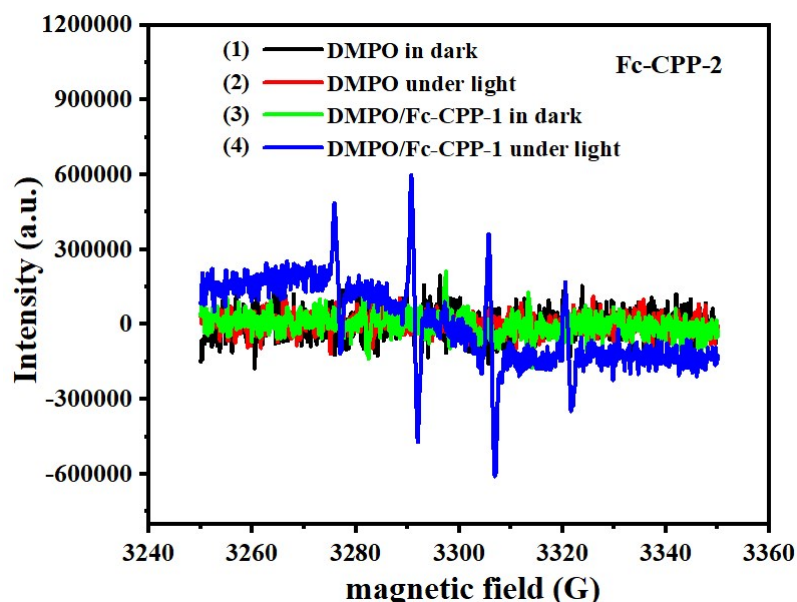


**Fig. S29** ESR spectra for DMPO-•OH in 1) distilled water of DMPO before irradiation, 2) distilled water of DMPO after irradiation, 2) distilled water of DMPO in the presence of Fc-CPP-2 before irradiation, and d) distilled water of DMPO in the presence of Fc-CPP-2 after irradiation. DMPO was used as spin adduct. Characteristic

four peaks of DMPO-•OH adduct (peak area = 1:2:2:1) are observed for Fc-CPP-2 under visible light irradiation, demonstrating •OH species are generated.

**Table S2** The content of hydrogen peroxide in the reaction system under different illumination times

Photocatalyst	H <sub>2</sub> O <sub>2</sub> /umol (5 min)	H <sub>2</sub> O <sub>2</sub> /umol (10 min)	H <sub>2</sub> O <sub>2</sub> /umol (15 min)
Fc-CPP-1	0.626	1.171	1.232
Fc-CPP-2	0.594	1.093	1.197

We have reported the procedure to quantify the hydrogen peroxide after the reaction (Section 2. Methods in supporting information), and conducted many experiments through this method. We tested the content of hydrogen peroxide in the reaction system under different illumination times, and the data is shown in Table S2. After 5 min, 10 min, and 15 min of irradiation, the amount of hydrogen peroxide in the reaction system of Fc-CPP-1 photocatalytic reduction of Cr(VI) is 0.062, 1.171 and 1.232 umol, respectively. In the case of Fc-CPP-1, after 15 min of continuous visible light illumination, the reduction ratio of Cr(VI) can reach up to 99%. Theoretically, the amount of hydrogen peroxide produced at this time is 1.514 umol. In fact, the amount (1.232 umol) detected in this manuscript is less than the expected theoretical value. The hydrogen peroxide is unstable under light conditions, we wonder if part of the hydrogen peroxide is decomposed into hydroxyl radicals (•OH) in the catalytic process, which makes the final detected amount smaller. Then electron spin resonance (ESR) spectroscopy were performed by employing 5,5-dimethyl-1-pyrroline N-oxide (DMPO) as a spin trapping agent to detect •OH. Characteristic four peaks of DMPO-•OH adduct (peak area = 1:2:2:1) are observed for Fc-CPPS under visible light irradiation, demonstrating •OH species are generated. Because part of the hydrogen peroxide will decompose into •OH species under light conditions, the amount of hydrogen peroxide detected will be smaller than theoretically. However, it should be noted that the generation of •OH is not caused by the oxidation of water, which require a potential of 2.38 vs NHE.<sup>1</sup> The LUMO potential of Fc-CPPs (1.78V vs Ag/AgCl/KCl(saturated) or 2.0 vs NHE) is not enough to oxidize water to •OH. Although the detected amount is slightly smaller than the theoretical value, it can be seen that the amount of hydrogen peroxide in the system is increasing with the prolonging of the illumination time, indicating that the redox reaction is proceeding smoothly.

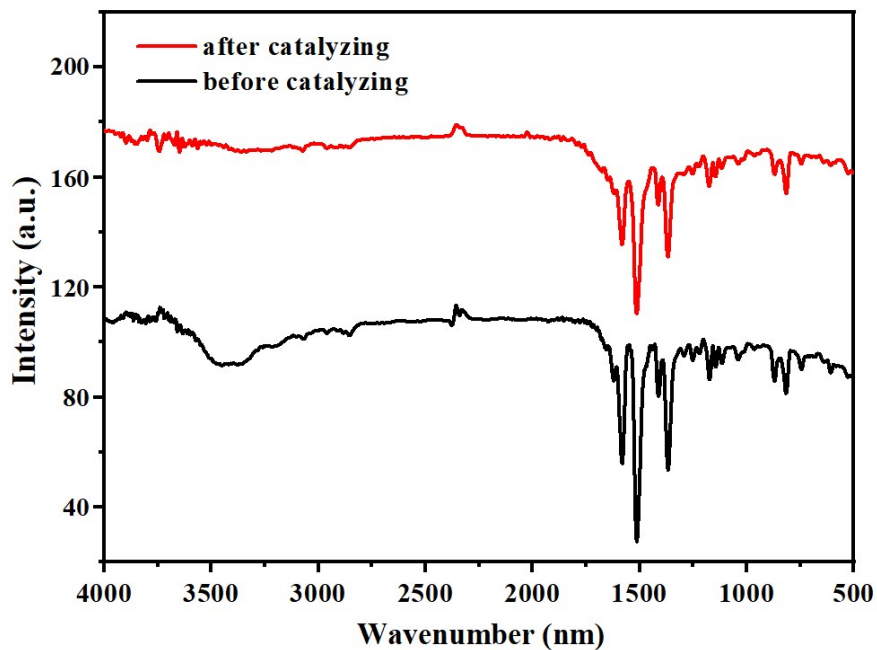


Fig. S30 FTIR spectra of Fc-CPP-1 before and after the photocatalytic reaction.

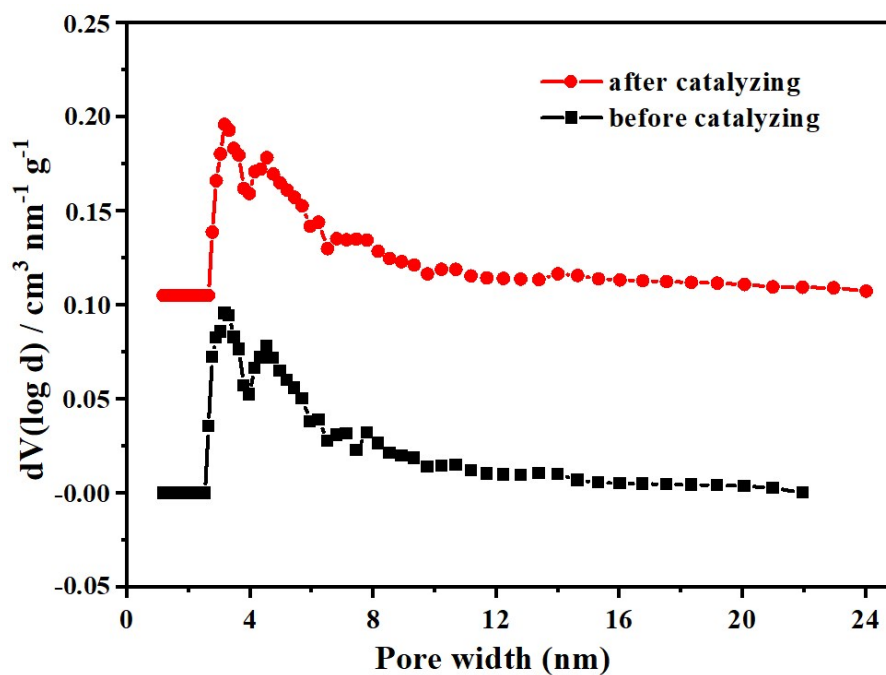


Fig. S31 Pore size distribution curves for Fc-CPP-1 before and after the photocatalytic reaction.

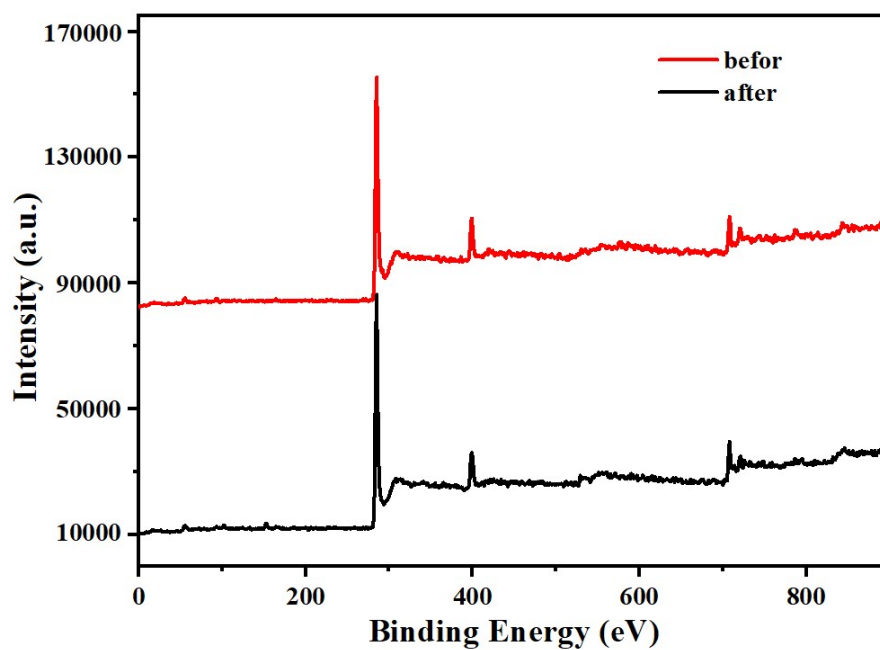


Fig. S32 XPS spectra of Fc-CPP-1 before and after the photocatalytic reaction.

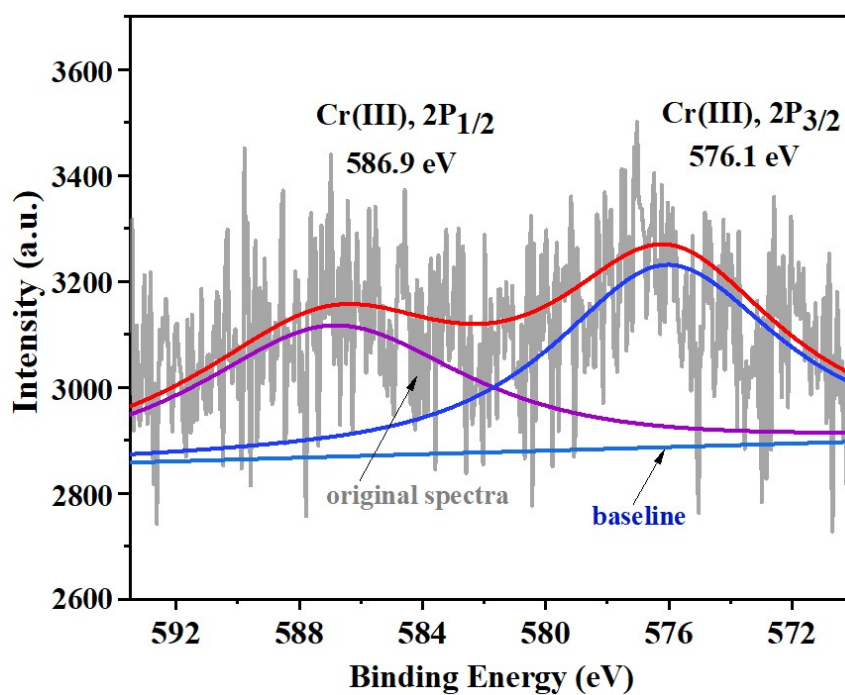


Fig. S33 XPS of Cr 2p spectra for Fc-CPP-1 after the photocatalytic reaction.

## References

1. Y. Nosaka and A. Y. Nosaka. *Chem. Rev.*, 2017, **117**, 11302–11336.